Research Square

Preprints are preliminary reports that have not undergone peer review.
They should not be considered conclusive, used to inform clinical practice,
or referenced by the media as validated information.

Leveraging the Redox Shuttle Effect of TEMPO for the reactivation of Dead Zinc in Aqueous Zinc-Ion Batteries

Qianhong Da
Yunnan Normal University
Zhengze Dang
Yunnan Normal University
Dan Liu
Yunnan Normal University
Ziyi Kang
Yunnan Normal University
Yunbo Zhang
zhangyunbo@ynnu.edu.cn
Yunnan Normal University
Peizhi Yang
Yunnan Normal University

Research Article

Keywords: zinc ion battery, dead zinc, TEMPO, redox mediator, reactivation

Posted Date: March 9th, 2026

DOI: https://doi.org/10.21203/rs.3.rs-8863777/v1

License: This work is licensed under a Creative Commons Attribution 4.0 International License.
Read Full License

Additional Declarations: No competing interests reported.

Abstract

Zinc metal anode plays a vital role in aqueous zinc-ion batteries, while the continuous formation of zinc dendrite and the resultant detached dead zinc hinder the real use. Herein, a dead zinc reusage strategy is proposed by utilizing the reaction of redox medium 2,2,6,6-tetramethylpiperidine-1-oxyl (TEMPO). The shuttle reaction of TEMPO during the cycling processes enabling the continuous reaction of dead zinc into the usable zinc ions. With the addition of TEMPO, Zn-Cu batteries have an average Coulomb efficiency of 99.34%. The Zn-MnO_2 full cell as well exhibits remarkable cycle stability during 1500 long cycles by adding TEMPO. This new approach proposed here to reactivate dead zinc promotes the advancement of the research of the long-life zinc metal batteries.

1. Introduction

Aqueous zinc-ion batteries (AZIBs) have emerged as one of the most promising candidates for next-generation energy storage systems, due to their high safety, low cost, and environmental friendliness, in contrast to lithium ion battery with flammable organic electrolyte.[1] In AZIBs, the zinc metal anode plays an irreplaceable role, since zinc metal has a high theoretical capacity (820 mAh g^{-1}) and a low standard redox potential (-0.76 V vs. standard hydrogen electrode) enabling efficient charge storage and transfer.[2–4] However, the real use of AZIBs is hindered by two yet solved problems: the continuous production of zinc dendrites, [5, 6]and the uncontrolled formation of side products ,e.g. hydrogen, ZnO, basic zinc salts),[7–9] on the anode interface. The dendrite issue is more sever in the cycling processes. Zinc dendrite will detach from the anode for the uneven stripping behavior, and lose electrical contact with the current collector, forming the inactive dead zinc, which cannot be used in the following electrochemical cycles.[10–13] The accumulation of dead zinc will accumulate gradually and increase the risk of short circuit and threaten the long-life safety of the batteries. These issues generally result in low Coulombic efficiency (CE), poor cycle stability, and short lifespan of AZIBs, limiting their commercialization.[14, 15]

Extensive researches have been conducted to develop strategies to solve the dendrite problems. The design of three-dimensional (3D) anode structures has been proven effective.[16–20] For example, a 3D porous zinc anode was fabricated using a template-assisted electrodeposition method.[21] The Increasing surface area lower local current density and the pore structure provides abundant zinc ion diffusion paths, guaranteeing the even deposition. It is also effective to modify the electrode interface with an artificial solid electrolyte interphase (SEI) layer, consisting of organic,[20–22] inorganic[25, 26] and organic-inorganic hybrid materials.[27, 28] The artificial SEI layer prevents the zinc anode from direct contacting with electrolyte, and thus suppress hydrogen evolution reaction (HER) and corrosion. It also allows selective transport of zinc ions to ensure the ion supply for the reaction.[29, 30] Electrolyte modification, including the addition of additives,[31, 32] tuning of salt concentration,[33, 34] or use of mixed solvents,[35, 36] has as well been proposed. For instance, the introduction of a small amount of aluminum trifluoride (AlF_3) into zinc trifluoromethanesulfonate ($Zn(CF_3SO_3)_2$) electrolyte can induce the formation of a stable SEI layer composed of ZnF_2 and Al_2O_3, significantly improving the cycle stability of zinc

anodes.[37] These works provide extensive strategies to improve the electrochemical performance of zinc metal anode, but most of them focus on preventing the formation of dead zinc rather than reactivating the already generated dead zinc, which has been proven as a vital role in the performance of zinc metal anode[38, 39]. Therefore, it is important to develop an efficient way to reactive dead zinc.

Some works have been done in the perspective of reactivation of dead zinc to further improve the performance of zinc metal anodes.[40, 13] Current strategies primarily rely on the introduction of redox media to react detached, inactive dead zinc into soluble, active zinc ions.[41, 42] For example, some studies have utilized transition metal ions (e.g., Cu^{2+}, Ni^{2+}) as redox shuttles—these ions can oxidize dead zinc (Zn^0) to Zn^{2+} through redox reactions,[43, 44] and the reduced metal ions (e.g., Cu^0, Ni^0) can then be oxidized back to their original states at the cathode, completing the redox cycle. Other approaches, such as the use of organic redox molecules (e.g., quinones, Ferrocene-derived compound, 7,8-dihydroxyphenazine-2-sulfonic acid) and iodide ions,[45, 46] have also been explored and the electrochemical performance is also improved but their poor stability in aqueous electrolytes and high solubility loss during cycles hinder their long-term performance. Therefore, there is an urgent need to develop a stable, compatible, and efficient redox medium that can realize the continuous reactivation of dead zinc while not interfering with the normal operation of AZIBs.

Here a novel strategy is proposed to reactive dead zinc by using the redox shuttle effect of 2,2,6,6-tetramethylpiperidine-1-oxyl (TEMPO). TEMPO is an organic molecule with excellent stability and reversible redox behavior in aqueous systems.[47] During the charge-discharge process of AZIBs, TEMPO undergoes a reversible redox reaction between TEMPO and $TEMPO^+$. TEMPO is oxidized to $TEMPO^+$ at the cathode. Then $TEMPO^+$ transports to anode side oxidizes dead zinc (Zn^0) to Zn^{2+}, and $TEMPO^+$ itself is then reduced back to TEMPO. This forming a continuous dead zinc reactivation cycle. The electrochemical performance of zinc-based batteries with TEMPO additives is thus improved for the elimination of dead zinc and dendrite accumulation. In Zn-Cu half-cells with the addition of TEMPO maintains an average Coulombic efficiency of 99.34% over even after 1000 cycles. In Zn-MnO_2 full cells, the battery achieved the cycle stability as long as 1500 cycles.

2. Materials and Methods

Zinc trifluoromethanesulfonate ($Zn(CF_3SO_3)_2$), 2,2,6,6-tetramethylpiperidine oxide (TEMPO), Super-P carbon black and PVDF were provided by Aladdin, and manganese dioxide (MnO_2) was provided by McLean. Ultrapure water used in all experiments was prepared by an ultrapure water production system.

All batteries were electrochemically tested using CR2025 button cells. Glass fiber membrane was used as a diaphragm. Zinc trifluoromethanesulfonate [$Zn(CF_3SO_3)_2$] was dissolved in ultrapure water to formulate a 2M $Zn(OTf)_2$ electrolyte. The TEMPO was configured in the 2M $Zn(OTf)_2$ electrode solution and sonicated at room temperature until completely dissolved.

Symmetric cells were assembled using bare zinc electrodes in the electrolyte (with or without the TEMPO additive). Half cells were assembled using bare zinc as the working electrode and copper foil as the counter electrode. The anode material was prepared by mixing MnO_2 with conductive carbon black and polyvinylidene fluoride (PVDF) binder in the ratio of 8:1:1 by mass with an appropriate amount of N-methylpyrrolidone (NMP), coating on 60 mm titanium foil, and drying at 120°C for 12h in vacuum. The full cell consisted of a bare zinc anode, a prepared MnO_2 cathode and an electrolyte with (ZF-TEMPO)or without TEMPO additive (ZF). The electrochemical performance of the above cells was evaluated on a LANDCT3002 battery test system. The half-wave potential of the electrolyte was measured on a CHI600E electrochemical workstation using a three-electrode setup. The cyclic voltammetry (CV) of TEMPO redox reaction was tested by three electrode system, in which a glassy carbon electrode was used as the working electrode, a platinum sheet as the counter electrode, and Ag/AgCl as the reference electrode. The full cell was tested by CV over a voltage range of 0.8–2.5 V. The electrolyte was then used as a reference electrode. Corrosion tests, electrochemical impedance spectroscopy (EIS) tests, and constant potential ammeter (CA) tests were performed on a Tatsumi electrochemical workstation. The frequency range of EIS was from 0.1 Hz to 1 MHz. Constant potential galvanometer tests were performed at an overpotential of -150 mV. The linear scanning voltammetry (LSV) method was used to measure the voltage of the different hydrogen precipitation potentials at the zinc anode in the same electrolyte at a scan rate of 0.5 m/s. The potential of hydrogen precipitation at the zinc anode in the different electrolytes was measured using linear scanning voltammetry (LSV). to 150 mV for Tafel testing of symmetric cells.

3. Results and Discussion

To clarify the functional principle of the TEMPO additive in regulating the zinc anode behavior and its mitigation of battery performance, Fig. 1 illustrates the working mechanism of the TEMPO additive. In the system without TEMPO addition (Fig. 1a), the uncontrolled zinc metal deposition and stripping results in the formation of dead zinc and the rapid growth of zinc dendrites, severely compromising battery performance. In contrast, TEMPO-modified electrolyte smoothens the surface zinc anode, as shown in Fig. 1b, since the oxidization reaction of TEMPO continuously produces $TEMPO^+$, which transfers to anode to convert dead zinc into active Zn^{2+}. The reactivation of dead zinc inhibits the accumulation of zinc dendrites and promotes the uniform deposition of zinc ions. To verify the redox reversibility of TEMPO in the electrolyte system, cyclic voltammetry (CV) tests were first conducted at a scan rate of 0.01 mV/s, and the results are presented in Fig. 1c. The CV curves show that the electrolyte containing TEMPO exhibits an oxidation peak located at 0.65 V and the reduction peak at 0.48 V, corresponding to the oxidization and reduction reaction of the TEMPO/$TEMPO^+$. This phenomenon indicates that TEMPO has excellent redox reversibility in the system. The *in-situ* UV-vis spectroscopy results further confirm that the production of $TEMPO^+$ in the working voltage range of aqueous zinc batteries. As shown in Fig. 1d, the maximum absorption peak of the TEMPO-modified electrolyte appears at 456 nm in the initial state, and this characteristic peak belongs to the Nitrogen-oxygen bond (N–O) structure in TEMPO. With the charging voltage increasing, the absorption peak position shifts left, and

reaches 443 nm at 2 V, corresponding to the formation of the nitrogen-oxygen double bond ($N^+=O$) in the $TEMPO^+$. Along with the shift in peak position, the absorbance of the system significantly decreased. This change was due to the lower molar extinction coefficient of $TEMPO^+$ compared to its radical form, further verifying the reversible conversion behavior of the TEMPO/$TEMPO^+$ redox couple during the electrode process.[48]

Since the nucleation mode of zinc directly determines the uniformity of the anode deposition layer, chronoamperometry (CA) tests were further conducted to study the zinc deposition behaviors. As shown in Fig. 2a, The CA curves reveal an essential difference in the nucleation mode of zinc between the blank electrolyte and the TEMPO-modified electrolyte. In the blank electrolyte, the current response decreases rapidly, which indicates that zinc ions undergo continuous two-dimensional surface diffusion. This two-dimensional diffusion leads to uneven zinc nucleation and persistent dendrite growth, due to the unregulated migration and deposition of zinc ions. In contrast, TEMPO-modified electrolyte maintains a stable current-time curve. This stability suggests that TEMPO suppresses the dendrite formation and promotes the formation of a dense, uniform metal deposition layer. The reason is that TEMPO additive regulates the ion migration rate and thus ensure uniform nucleation and deposition of zinc. The improvement of the electrochemical behaviors can be also attributed to the better wettability of TEMPO-modified electrolyte. As shown in **Figure S1a**, the contact angle of the electrolyte without TEMPO is 71.42°, while that of the electrolyte containing TEMPO is 63.45°in **Figure S1b**. The less contact angle has a positive effect on the uniform deposition. To assess the effect of TEMPO on suppressing the self-corrosion of the zinc anode, Tafel analysis based on linear polarization curve tests was carried out. Figure 2b shows that the corrosion current density of the TEMPO-modified electrolyte is lower than that of the blank electrolyte system. This phenomenon indicates that TEMPO can effectively delay the self-corrosion process of the zinc anode. TEMPO consumes the active oxides that cause corrosion and forms a protective layer on the metal surface. This protective layer blocks the continuous erosion of the zinc anode by the electrolyte, thereby reducing the corrosion current density.

X-ray diffraction (XRD) tests were conducted on zinc electrodes after 50 cycles to explore the effect of TEMPO on the crystal structure. Figure 2c displaying the XRD patterns shows that the TEMPO-modified electrolyte has the effect on the elimination of dead zinc. The zinc deposits in the both electrolytes exhibit the preferred growth of (002), (100), and (101) crystal planes. The deposited layer in the TEMPO-containing system maintains a pure zinc crystal structure. Additionally, quantitative analysis of crystal orientation shows that the ratio of the intensities of (002) to (101) crystal plane in the blank TEMPO system is 0.87, while that in the TEMPO-modified electrolyte is only 0.53. It indicates that in the TEMPO-modified electrolyte, the (002) plane is the main site for deposition. The reason for this crystallographic regulation is that TEMPO redox reactions consume dead zinc and the side reaction products at anode. Hence, the TEMPO-modified electrolyte promotes the ordered deposition of zinc atoms and adjusts the preferred orientation of crystal planes to suppress dendrite accumulation.

To gain more understandings of the suppression effect of TEMPO additive on the disordered growth of zinc dendrites and side reactions, the surface of Cu was characterized using scanning electron

microscopy (SEM) under different area capacities (Fig. 2d-i). In the blank electrolyte, as the capacity increased from 5 $mAhcm^{-2}$ to 15 $mAhcm^{-2}$, uneven deposition of zinc could be observed (Fig. 2d-f). In contrast, in the TEMPO-modified electrolyte, uniform and flat surface deposition could be observed (Fig. 2g-i).

To evaluate the reactivation effect of TEMPO visually, dead zinc was added into electrolyte with and without $TEMPO^+$. TEMPO of 10 mM was added to the electrolyte and charged to produce $TEMPO^+$. Within 15 minutes, the silver-gray dead zinc powders dissolved, indicating that the dead Zn could be oxidized by $TEMPO^+$ and form soluble Zn^{2+} substances in the solution (Fig. 3a). In contrast, after being immersed in pure electrolyte and TEMPO-ZF electrolyte for 15 minutes, the dead Zn precipitate remained intact (Fig. 3b). Figure 3c shows the in situ changes of the absorption peaks of UV/Vis spectra of $TEMPO^+$ electrolyte. The red shift of the peaks indicates that the oxidized $TEMPO^+$ was reduced gradually by the dead Zn to TEMPO. To evaluate the effect of TEMPO on the reversibility of the zinc anode, Zn-Cu half-cell cycling tests were conducted at a current density of 4 mA cm^{-2} and the plating capacity of 4 mAh cm^{-2}. Figure 3d presents the charging-discharging curves of Zn-Cu batteries. It shows the stripping capacity of the cell with the TEMPO-modified electrolyte is significantly higher than that of the cell with the blank electrolyte. The excellent reversibility and high stripping capacity of the TEMPO-modified system are due to the ability of TEMPO redox shuttles to continuously reactivate dead lithium, ensuring sufficient active material for cycling and thus maintaining stable CE. The CE stability test of the Zn-Cu cell shown in Fig. 3e indicates that the Zn-Cu cell using the blank electrolyte fails after 200 electroplating/stripping cycles and CE fluctuates significantly. This failure is caused by the continuous accumulation of dead zinc and dendrites. In contrast, the cells with TEMPO-modified electrolyte maintains an average CE of 99.5% over 1000 cycles. To closely investigate the electrochemical behaviors, Fig. 3f shows the voltage-to-capacity curves after 5, 25, and 50 cycles in the original electrolyte. By the 50th cycle, capacity had significantly degraded and overpotentials had increased. In contrast, the battery exhibited markedly improved cycling stability in the TEMPO-modified system (Fig. 3g). Even at the 800th cycle, the charge-discharge curve maintains a relatively stable voltage plateau. Further comparison of overpotential changes (insets in Figs. 3f and 3g) reveals that the battery with TEMPO-modified system exhibits an overpotential of 90.6 mV at the 800th cycle. This value remains essentially unchanged compared to the 200th cycle (84.2 mV), 400th (81.1 mV), and 600th cycles (80.4 mV), showing little change. This contrasts sharply with the original electrolyte battery, where the overpotential increased from 121.7 mV at the 5th cycle to 147.6 mV. The lower electrochemical polarization, superior cycling stability, and extended lifespan demonstrate that TEMPO plays a crucial role in regulating zinc deposition behavior and enhancing battery performance.

To verify the practical application value of the TEMPO-modified electrolyte, a full battery with manganese dioxide (MnO_2) as the cathode was assembled, and its electrochemical performance was tested as shown in Fig. 4. Figure 4a presents the CV curves of the Zn-MnO_2 battery. The CV curves show that compared to the blank electrolyte, the cells with the TEMPO-modified electrolyte exhibits an oxidation peak at 1.73 V and 1.61V and reduction peaks at 1.31 V and 1.28 V, suggesting the good reversibility of

the electrochemical reactions in Zn-MnO_2 cells. This higher redox peaks indicate a more reversible electrochemical process in the TEMPO-modified system. The improved reversibility is because of the elimination of dead zinc by the redox reactions of TEMPO. Rate performance tests were also conducted, and the results are shown in Fig. 4b. The results indicate that at various current densities, the specific capacity of the battery with the TEMPO-modified electrolyte is higher than that of the battery using the blank electrolyte. This improvement in rate performance suggesting reactivation effect of dead lithium by TEMPO exists at various current densities. **Figure S2** a and b respectively show the electrochemical curves of the Zn-MnO_2 battery prepared with the basic electrolyte and the electrolyte containing TEMPO. During the cycling tests, compared with the basic electrolyte, the charging and discharging curves of the battery with TEMPO exhibited higher capacity, and the charging and discharging curves showed similar characteristics, indicating that its electrolysis/exfoliation behavior remained good. Electrochemical Impedance Spectroscopy tests were conducted to further prove the dead lithium reactivation effect of TEMPO and The EIS curves of the Zn-MnO_2 battery after 50 cycles are shown in Fig. 4c. It was found that the interface resistance of the TEMPO-modified system is lower than that of the blank electrolyte system. This impedance difference results from the inhibition effect of TEMPO on the accumulation of dead zinc. Dead lithium accumulation layer will increase the interface resistance, since it blocks the ion transport and enlarges anode surface area leading to severe side reaction. TEMPO continuously reactive dead zinc in batteries and thus maintain a low-resistance interface.

To evaluate the long-cycle stability of the Zn-MnO_2 battery with the TEMPO-modified electrolyte, cycling tests were conducted at a current density of 4 A g^{-1}. Figure 4d shows the electrochemical curves of Zn-MnO_2 battery with the addition of TEMPO. In the long-term cycling tests, the charging and discharging curves keep the similar features, suggesting its well-maintained plating/stripping behaviors. Figure 4e shows the long-cycle performance of the Zn-MnO_2 battery. Even after 1500 cycles, the specific capacity of the battery with the blank electrolyte decreased from 138.4 mAh g^{-1} to 20 mAh g^{-1}, showing an obvious capacity decay. In contrast, the battery with TEMPO addition exhibited better stability, with the specific capacity dropping from 146.6 mAh g^{-1} to 68 mAh g^{-1}.

Scanning electron microscopy (SEM) was used to observe the surface morphology of the zinc anodes after 500 cycles, and the results are shown in Fig. 5a-d. The SEM images in Fig. 5a shows the surface morphology of the zinc anode in blank electrolyte, and uneven deposits were observed. In its zoomed images (Fig. 5b), the deposits were needle-like shape, which is the typical morphology of dendritic zinc[49]. Figure 5c, d are the images of surface morphologies of zinc anode in the TEMPO-modified electrolyte with different magnifications, which clearly show the zinc electrode surface was flat without dendrite formation. The excellent long-cycle stability and the smooth sur anode morphology in the TEMPO-modified system are attributed to dead zinc reactivation by TEMPO redox reactions. Without the accumulation of uncontrolled dendritic deposits, the electrolyte consumption and ion transport blockage are largely mitigated, leading to improved electrochemical performance. XPS further investigated the surface chemistry of the zinc anode in both blank and TEMPO-modified electrolyte after cycling tests, and the results are shown in Fig. 5e-h. The XPS spectra of C1s of the both zinc anodes (Fig. 5e, f)

indicate the existence of typical C-C (284.8 eV), O-C = C (288.5 eV) and -CF_3 (293.0 eV) bonds. But intensities of peaks corresponding to O-C = C and -CF_3 bonds are significantly increase for the anode of TEMPO-modified electrolyte, indicating more carbonyl groups and F-rich organic compounds produced on the surface of anode. The Zn2p spectrum of zinc anode in blank electrolyte shown in Fig. 5g exhibits mainly the information of zinc metal, while in Zn2p spectrum of zinc anode in TEMPO-modified electrolyte (Fig. 5h), there exist ZnO and ZnF_2 peaks, indicating the more oxidized state of the surface. The F-rich and more oxidized surface of anode benefit the robust interface and even plating zinc metal, which improves the electrochemical performance of batteries along with the reactivation effect of TEMPO.

In conclusion, this work aims to address the dead zinc issues in zinc metal batteries and proposes a novel strategy by using the redox shuttle effect of 2,2,6,6-tetramethylpiperidin-1-oxyl (TEMPO) to reactivate dead zinc. TEMPO can be oxidized at cathode producing $TEMPO^+$, which at anode reacts with dead zinc to produce usable zinc ions. The reversible redox reaction of TEMPO continuously reactive electrically isolated dead zinc, and inhibits dendrite accumulation on anode surface in cycling processes. With the addition of TEMPO in electrolyte, The Zn-Cu half-cell keeps stable electrochemical performance as long as 1000 cycles. The cycling stability of the Zn-MnO_2 batteries with TEMPO is largely improved to 1500 cycles. This TEMPO reactivation effect of dead zinc push forward the in-dept theoretical understanding of zinc metal anode and real-use process of aqueous zinc-based batteries.

Declarations

Acknowledgements

This work was financially supported by the National Natural Science Foundation of China (NSFC) Youth Fund (Grant No. 52202312), Yunnan Provincial Basic Research Program (General Program) (Grant No. 202301AT070076), Yunnan Provincial Special Program for Building a Science and Technology Innovation Center Facing South and Southeast Asia (Grant No. 202403AP140015)

Conflicts of interest

The authors declare that there are no conflicts of interest.

References

1. Liu K, Liu Y, Lin D, Pei A, Cui Y (2018) Sci Adv 4(6):eaas9820
2. Xie W, Zhu K, Yang H, Yang W (2024) Adv Mater 36:2306154
3. Wan F, Niu Z (2019) Angew Chem 131:16508
4. Service RF (2021) Science 372:890
5. Yang Q, Li Q, Liu Z, Wang D, Guo Y, Li X, Tang Y, Li H, Dong B, Zhi C (2020) Adv Mater 32:2001854
6. Lu W, Xie C, Zhang H, Li X (2018) *ChemSusChem 11*, 3996

7. Wan J, Wang R, Liu Z, Zhang L, Liang F, Zhou T, Zhang S, Zhang L, Lu Q, Zhang C, Guo Z (2023) ACS Nano 17:1610
8. Lin X, Zhou G, Liu J, Robson MJ, Yu J, Wang Y, Zhang Z, Kwok SCT, Ciucci F (2021) Adv Funct Mater 31:2105717
9. Cao L, Li D, Hu E, Xu J, Deng T, Ma L, Wang Y, Yang X-Q, Wang C (2020) J Am Chem Soc 142:21404
10. Nie C, Wang G, Wang D, Wang M, Gao X, Bai Z, Wang N, Yang J, Xing Z, Dou S (2023) Adv Energy Mater 13:2300606
11. Pu SD, Hu B, Li Z, Yuan Y, Gong C, Ning Z, Chau C, Yang S, Zhang S, Pi L, Tang YT, Yue J, Marrow TJ, Gao X, Bruce PG, Robertson AW (2023) *Joule 7*, 366
12. Yu X, Li Z, Wu X, Zhang H, Zhao Q, Liang H, Wang H, Chao D, Wang F, Qiao Y, Zhou H, Sun S-G (2023) *Joule 7*, 1145
13. Qian X, Chen T, Wang Y, Zhang Q, Li W, Fu J (2025) Angew Chem Int Ed 64:e202412989
14. Hu P, Zhu T, Wang X, Zhou X, Wei X, Yao X, Luo W, Shi C, Owusu KA, Zhou L, Mai L (2019) Nano Energy 58:492
15. Zhang N, Cheng F, Liu Y, Zhao Q, Lei K, Chen C, Liu X, Chen J (2016) J Am Chem Soc 138:12894
16. Yoo D, Kim KJ, Choi JW (2018) Adv Energy Mater 8:1702744
17. Jang J, Shin J, Ko S, Park H, Song W, Park CB, Kang J (2022) Adv Energy Mater 12:2103955
18. Mu Y, Li Z, Wu B, Huang H, Wu F, Chu Y, Zou L, Yang M, He J, Ye L, Han M, Zhao T, Zeng L (2023) Nat Commun 14:4205
19. Sun M, Sun Y, Wang N, Hu L, Ren X, Jia C, Li Z (2024) J Colloid Interface Sci 656:440
20. Chen J, Wang Y, Tian Z, Zhao J, Ma Y, Alshareef HN (2024) *InfoMat 6*, e12485
21. Ma L, Pollard TP, Zhang Y, Schroeder MA, Ren X, Han KS, Ding MS, Cresce AV, Atwater TB, Mars J, Cao L, Steinrück H-G, Mueller KT, Toney MF, Hourwitz M, Fourkas JT, Maginn EJ, Wang C, Borodin O, Xu K (2022) One Earth 5:413
22. Liu X, Wang X, Yao J, Li J, Gan Y, Wu Z, Zheng J, Hao W, Lv L, Tao L, Zhang J, Wang H, Ji X, Wan H, Wang H (2024) Adv Energy Mater 14:2400090
23. Pan S, Han J, Wang Y, Li Z, Chen F, Guo Y, Han Z, Xiao K, Yu Z, Yu M, Wu S, Wang D, Yang Q (2022) Adv Mater 34:2203617
24. Wang N, Chen X, Wan H, Zhang B, Guan K, Yao J, Ji J, Li J, Gan Y, Lv L, Tao L, Ma G, Wang H, Zhang J, Wang H (2023) Adv Funct Mater 33:2300795
25. Lian X, Ju Z, Li L, Yi Y, Zhou J, Chen Z, Zhao Y, Tian Z, Su Y, Xue Z, Chen X, Ding Y, Tao X, Sun J (2024) Adv Mater 36:2306992
26. Chen C, Liang Q, Wang G, Liu D, Xiong X (2022) Adv Funct Mater 32:2107249
27. Zhou K, Qi B, Liu Z, Wang X, Sun Y, Zhang L (2024) Adv Funct Mater 34:2411671
28. Mu T, Lu H, Wang H, Wang Y, Lou S, Zhang Y, Gao J, Ma Y, Zuo P, Zhu X, Yin G (2025) Nano Energy 138:110835

29. Tian H, Feng G, Wang Q, Li Z, Zhang W, Lucero M, Feng Z, Wang Z-L, Zhang Y, Zhen C, Gu M, Shan X, Yang Y (2022) Nat Commun 13:7922
30. Zhang Y, Howe JD, Ben-Yoseph S, Wu Y, Liu N (2021) ACS Energy Lett 6:404
31. Li J, Guo Z, Wu J, Zheng Z, Yu Z, She F, Lai L, Li H, Chen Y, Wei L (2023) Adv Energy Mater 13:2301743
32. Cao J, Zhang D, Yue Y, Chanajaree R, Wang S, Han J, Zhang X, Qin J, Huang Y (2022) Nano Energy 93:106839
33. Jiang Y, Wan Z, He X, Yang J (2023) Angew Chem Int Ed 62:e202307274
34. Qian L, Zhu H, Qin T, Yao R, Zhao J, Kang F, Yang C (2023) Adv Funct Mater 33:2301118
35. Ni G, Sun M, Hao Z, Zou G, Cao F, Qin L, Chen W, Zhou C (2023) Mater Today Energy 31:101204
36. Naveed A, Li G, Ali A, Li M, Wan T, Hassan M, Wang X, Ye P, Li X, Zhou Y, Su M, Guo R, Liu Y, Xu H, Chu D (2023) Nano Energy 107:108175
37. Wei Y, Wang B, Qian Z, Pan H, Peng Z, Sun Y, Yao X (2025) Small Methods e01277
38. Fang C, Li J, Zhang M, Zhang Y, Yang F, Lee JZ, Lee M-H, Alvarado J, Schroeder MA, Yang Y, Lu B, Williams N, Ceja M, Yang L, Cai M, Gu J, Xu K, Wang X, Meng YS (2019) Nature 572:511
39. Liu Y, Zhang F, Wang Z, Deng L, Dong L, Song K-P, Wang S, Liu H, Chen H (2024) Energy Storage Mater 65:103180
40. Zhao Y, Hong H, Zhong L, Zhu J, Hou Y, Wang S, Lv H, Liang P, Guo Y, Wang D, Li P, Wang Y, Li Q, Cao SC, Li H, Zhi C (2023) Adv Energy Mater 13:2300627
41. Wen Z, Fang W, Wu X, Qin Z, Kang H, Chen L, Zhang N, Liu X, Chen G (2022) Adv Funct Mater 32:2204768
42. Huang S, Yuan Z, Salla M, Wang X, Zhang H, Huang S, Lek DG, Li X, Wang Q (2023) Energy Environ Sci 16:438
43. Zhu Q, Cheng M, Zhang B, Jin K, Chen S, Ren Z, Yu Y (2019) Adv Funct Mater 29:1905979
44. Ji J, Yao J, Xu Y, Wan H, Zhang B, Lv L, Li J, Wang N, Zheng Z, Zhang J, Ma G, Tao L, Wang H, Wang Y, Wang H (2023) ENERGY Environ Mater 6:e12340
45. Mao J, Iocozzia J, Huang J, Meng K, Lai Y, Lin Z (2018) Energy Environ Sci 11:772
46. Wang S, Zhao Y, Lv H, Hu X, He J, Zhi C, Li H (2024) Small 20:2207664
47. Bergner BJ, Schürmann A, Peppler K, Garsuch A, Janek J (2014) J Am Chem Soc 136:15054
48. Zhang Y, Liu J, Li Y, Zhao D, Huang W, Zheng Y, Zhou J, Zhu C, Deng C, Sun Y, Qian T, Yan C (2023) Adv Funct Mater 33:2301332
49. Zhang D, Miao L, Song Z, Zheng X, Lv Y, Gan L, Liu M (2024) Energy Fuels 38:12510

Figures

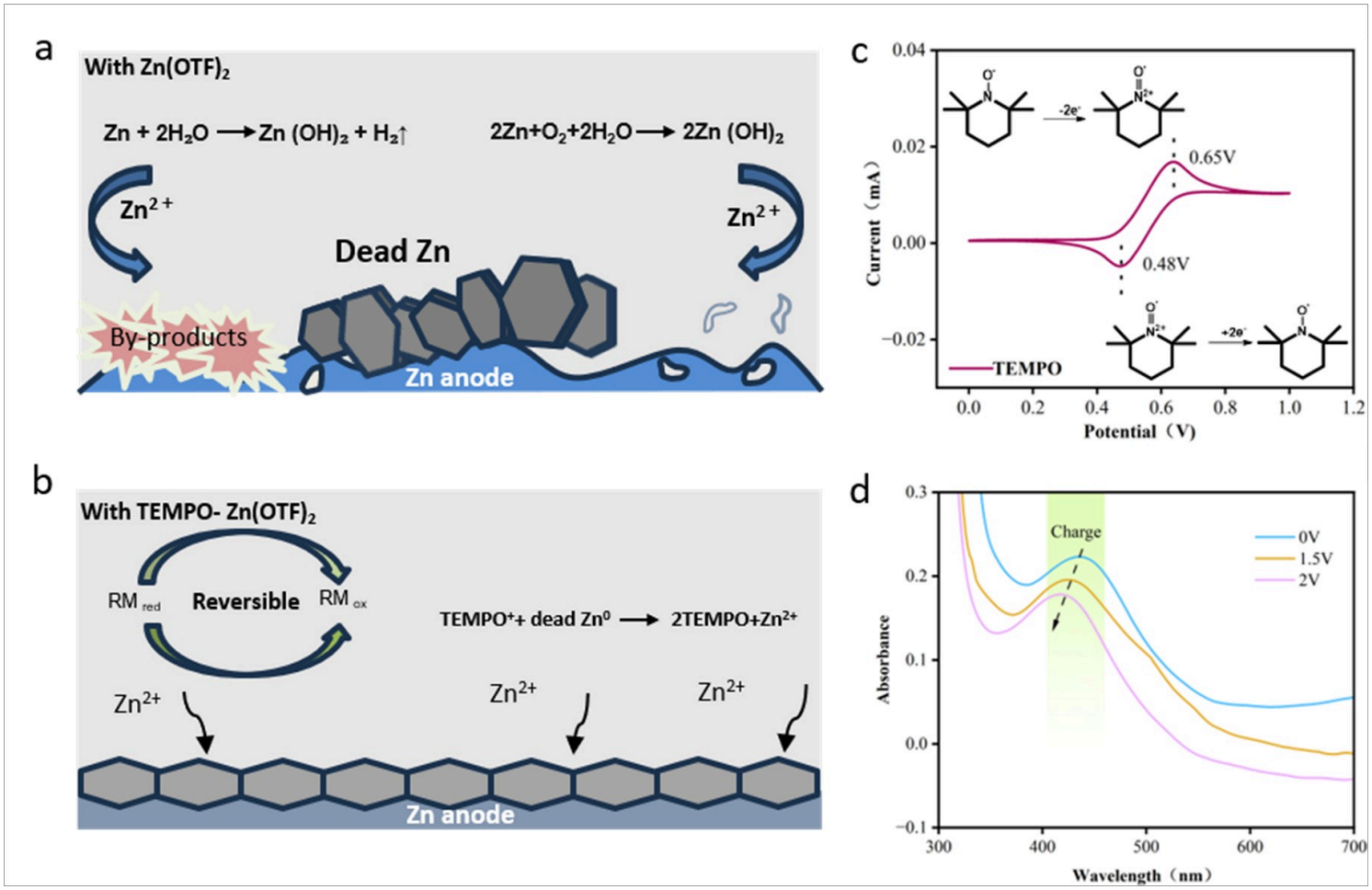


Figure 1

Schematic representation of Zn deposition mechanism in TEMPO-modified electrolyte a) without TEMPO and b) with TEMPO. c) Cyclic Voltammetry of the Zn-MnO_2 battery. d) In situ ultraviolet-visible spectroscopy of the TEMPO-modified electrolyte measured during the charging process.

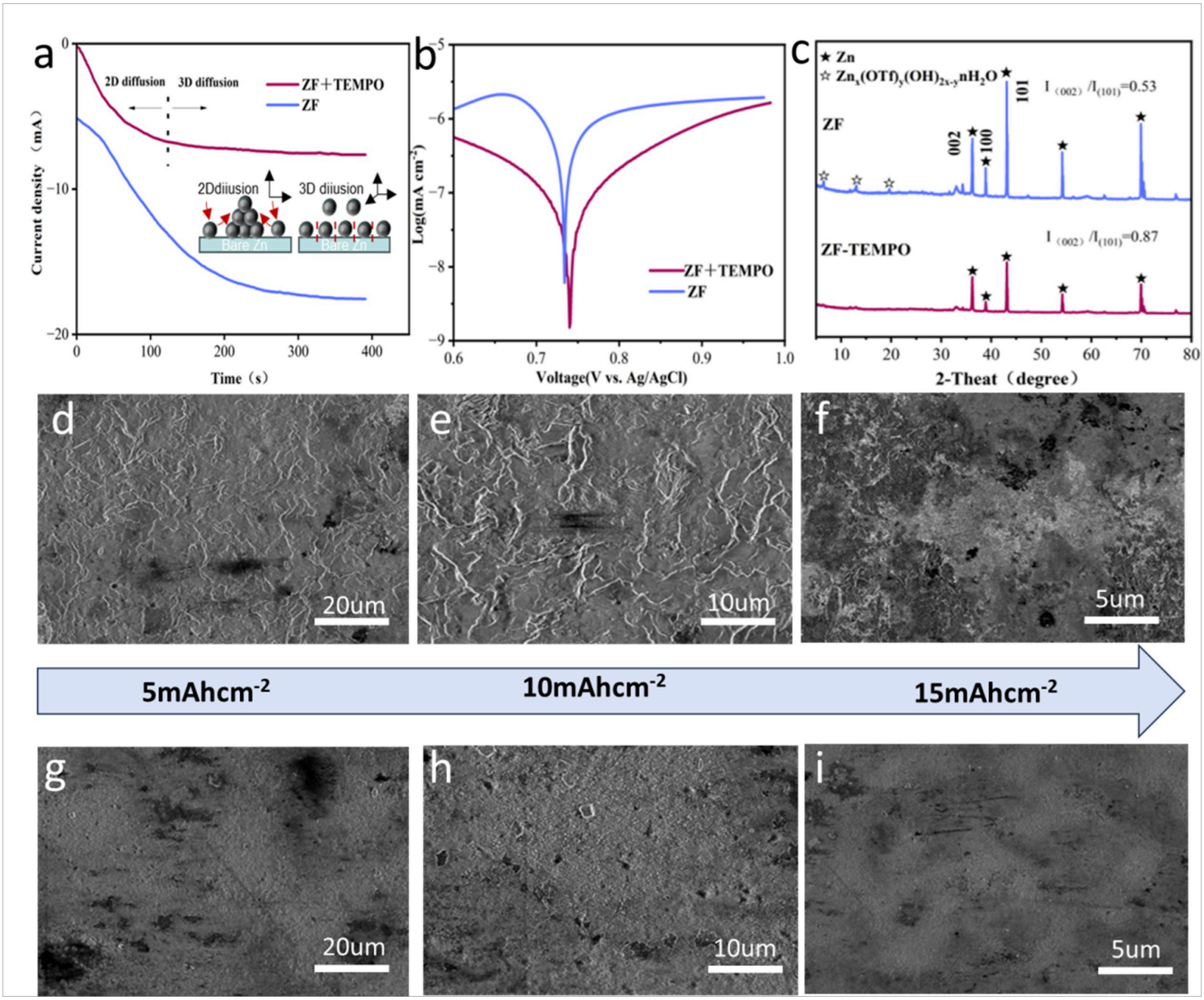


Figure 2

a) Time-domain amperometric test of zinc symmetric cells in electrolytes containing or not containing TEMPO additives under a constant overpotential of -150 mV. b) Linear polarization curves of zinc symmetric cells in different electrolytes. c) X-ray diffraction patterns of zinc electrodes in different electrolytes after 50 cycles. SEM images of the zinc deposits on Cu foil surface in Zn-Cu half-cell with the blank electrolyte under a plating capacity of d) 5 mAh cm^{-2}. e) 10 mAh cm^{-2}, f) 15 mAh cm^{-2}. SEM images of the zinc deposits on Cu foil surface in Zn-Cu half-cell with the TEMPO-modified electrolyte under a plating capacity of g) 5 mAh cm^{-2}, h) 10 mAh cm^{-2}, i) 15 mAh cm^{-2}.

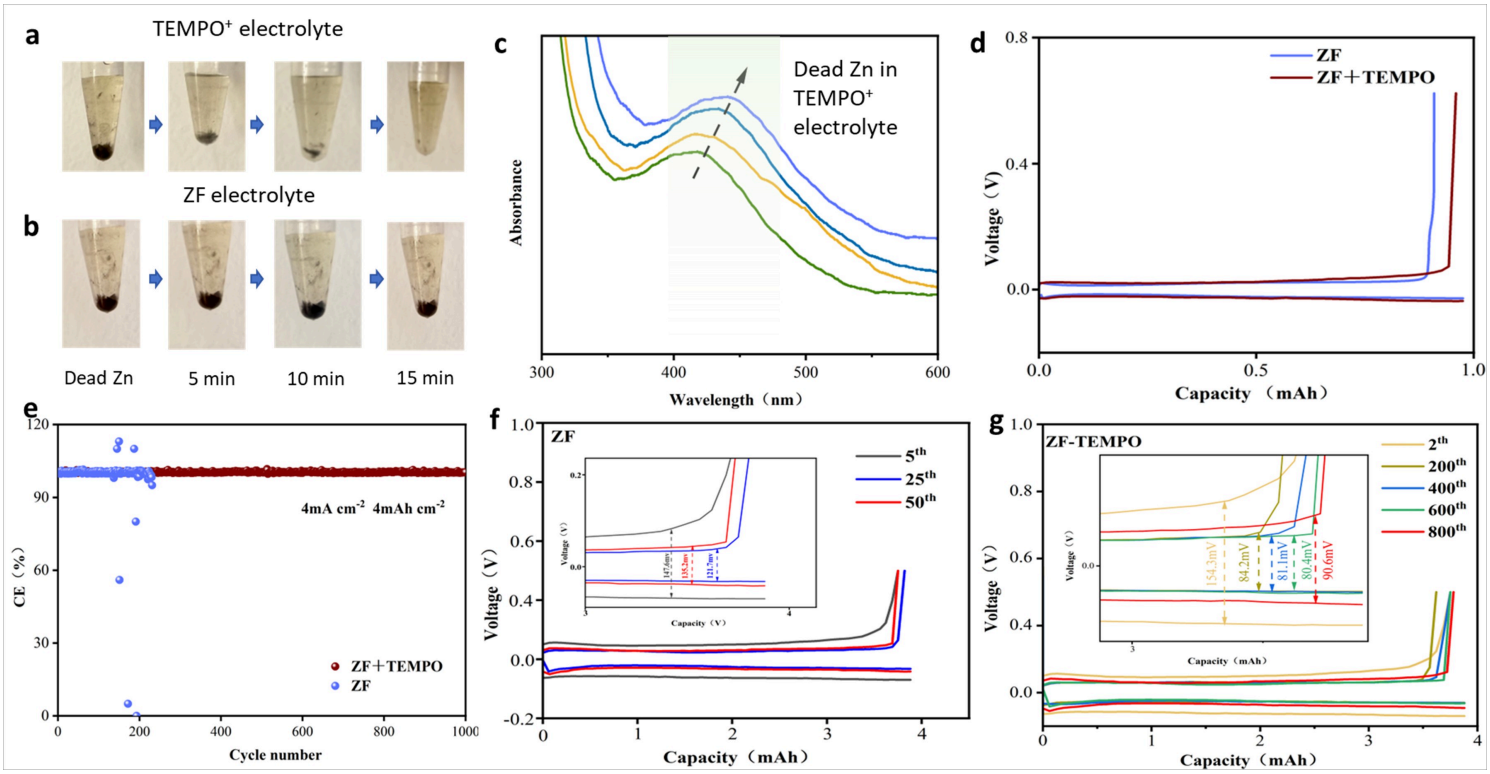


Figure 3

a) Comparison of CE performance of Zn-Cu batteries. b) Voltage distribution diagram of Zn-Cu batteries. c) Charge and discharge curves of Zn-Cu batteries in $Zn(OTF)_2$ electrolyte. d) Charge and discharge curves of Zn-Cu batteries in TEMPO-modified electrolyte.

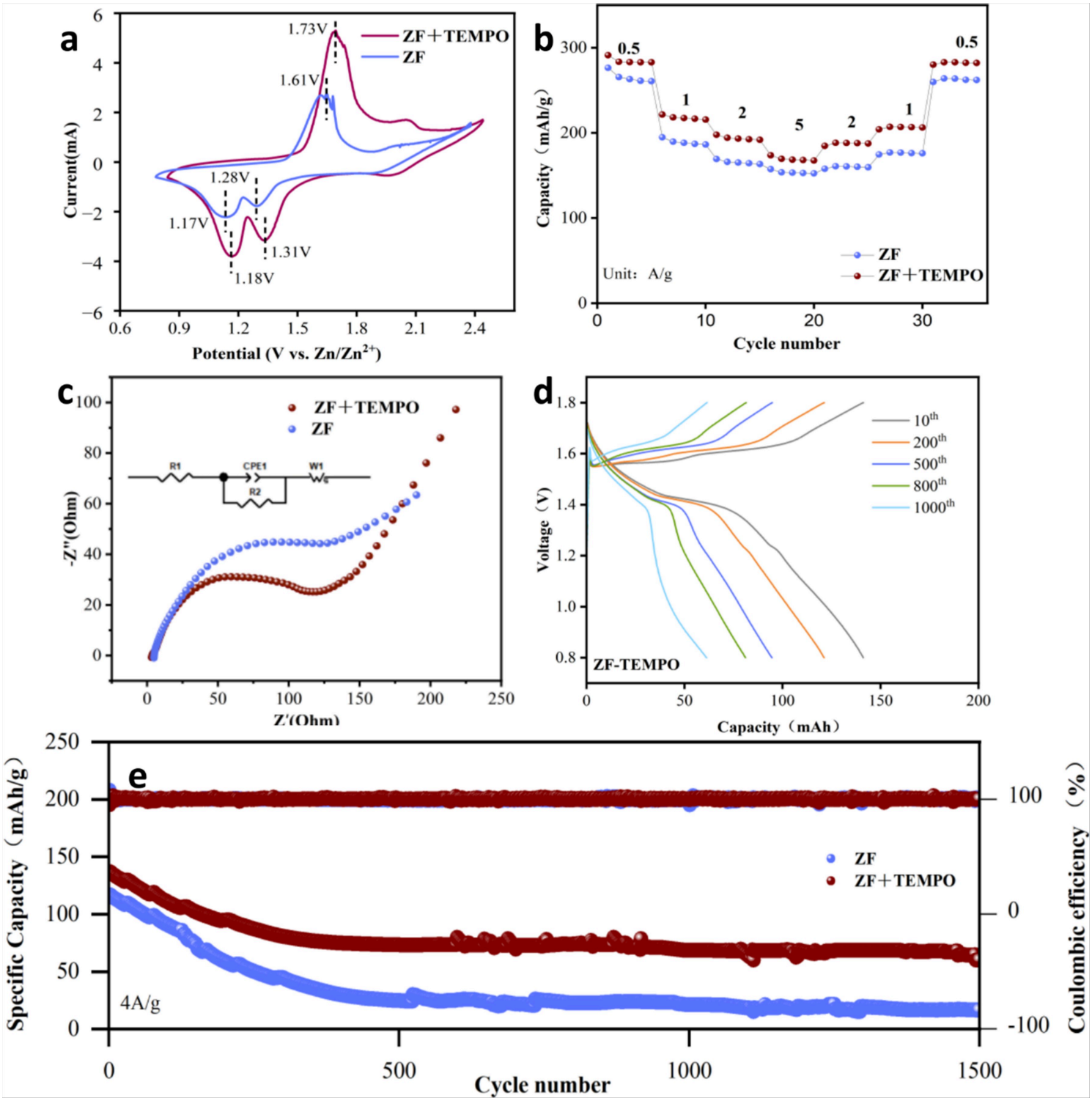


Figure 4

a) Electrochemical performance of the Zn-MnO_2 battery. b) Rate performance CV curve. c) EIS curve. d) Voltage-capacity distribution map of TEMPO-modified electrolyte at different current densities. e) Cycling performance of Zn-MnO_2 all-cell under 4A g^{-1} current density with different electrolytes.

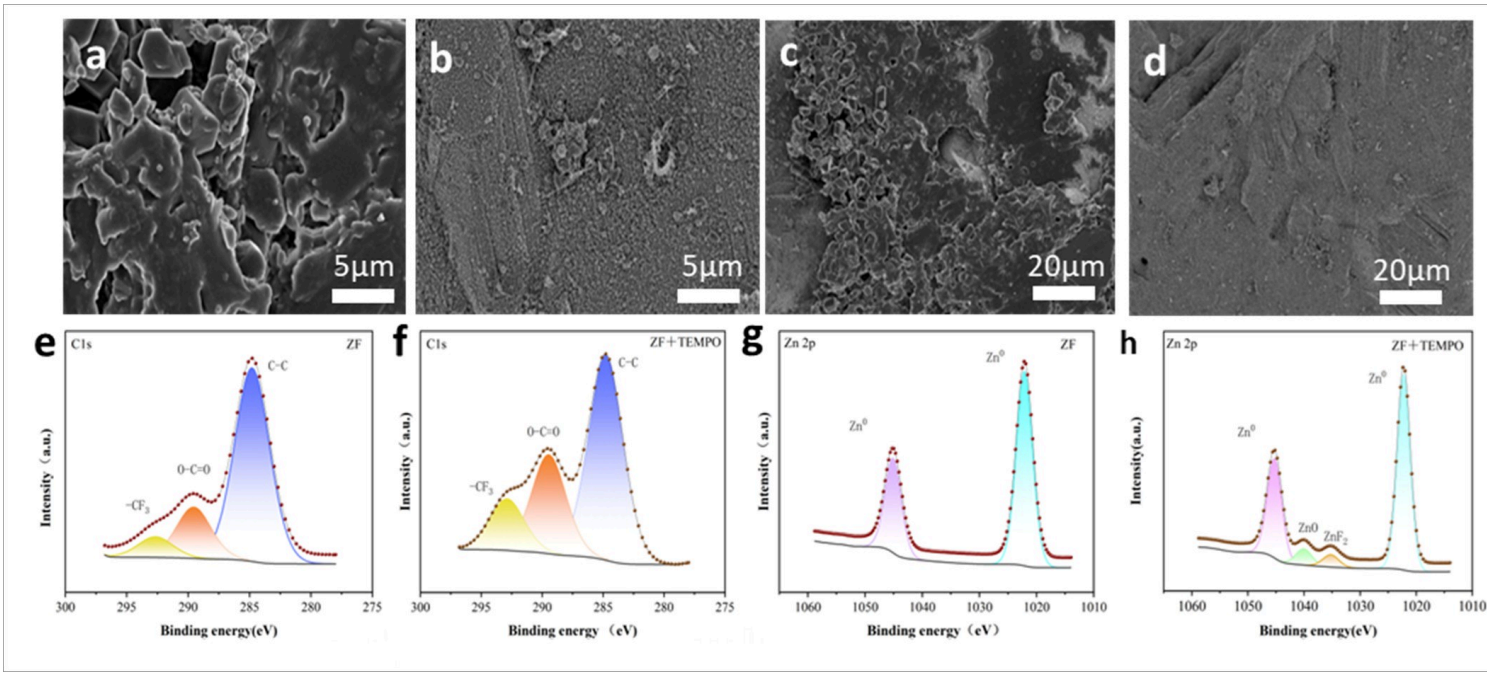


Figure 5

SEM images of the $Zn(OTF)_2$ and TEMPO-modified electrolytes after cycling. a), c) SEM images of the zinc surface of the Zn-MnO_2 battery after 500 cycles without adding TEMPO. b), d) SEM images of the zinc surface of the Zn-MnO_2 battery after 500 cycles with adding TEMPO. XPS of Zn anode surface after 100 h of cycling in $Zn(OTF)_2$ and TEMPO-modified electrolytes. e), f) C1s, g),h) Zn2p

Supplementary Files

This is a list of supplementary files associated with this preprint. Click to download.

- SupportingInformation.docx